Geophysical Research Letters

RESEARCH LETTER
10.1029/2022GL102124

# Emergent Constrained Projections of Mean and Extreme Warming in China

**Ziming Chen[1,2,3], Tianjun Zhou[1,2], Xiaolong Chen[1], Wenxia Zhang[1], Meng Zuo[1], Wenmin Man[1], and Yun Qian[3]**

[1]LASG, Institute of Atmospheric Physics, Chinese Academy of Sciences, Beijing, China, [2]College of Earth and Planetary Sciences, University of Chinese Academy of Sciences, Beijing, China, [3]Atmospheric Sciences and Global Change Division, Pacific Northwest National Laboratory, Richland, WA, USA

**Key Points:**

- Mean warming (2.98°C) in Coupled Model Intercomparison Project Phase 6 simulations are likely warmer than expected under an intermediate scenario in 2080–2099, given past warming
- Constraining on only the climate projection which is consistent with past warming, indicate a 0.65°C reduction in magnitude of mean warming
- Land area (population) witnessing daily maximum temperature warming greater than twice the standard deviation is 78% (85%) of raw projections

**Supporting Information:**

Supporting Information may be found in the online version of this article.

**Correspondence to:**

T. Zhou,
zhoutj@lasg.iap.ac.cn

**Citation:**

Chen, Z., Zhou, T., Chen, X., Zhang, W., Zuo, M., Man, W., & Qian, Y. (2023). Emergent constrained projections of mean and extreme warming in China. *Geophysical Research Letters*, *50*, e2022GL102124. https://doi.org/10.1029/2022GL102124

Received 18 NOV 2022
Accepted 17 SEP 2023

**Author Contributions:**

**Conceptualization:** Tianjun Zhou, Yun Qian
**Formal analysis:** Ziming Chen
**Funding acquisition:** Tianjun Zhou
**Investigation:** Ziming Chen, Tianjun Zhou
**Methodology:** Ziming Chen, Tianjun Zhou, Yun Qian
**Project Administration:** Tianjun Zhou
**Resources:** Tianjun Zhou



**Abstract** Reliable regional temperature projections including heat extremes are essential for climate change adaptation and mitigation. Taking China as an example, simple averages from Coupled Model Intercomparison Project Phase 6 (CMIP6) models project high warming due to sampling many high climate sensitivities in the ensemble. Here, we develop an emergent constraint (EC) framework to obtain constrained mean and daily maximum temperature (TXx) warming over China by using observed global warming and local residual warming. The constrained annual mean and TXx warming over China (2.33°C [1.61–3.05°C] and 2.31°C [1.21–2.99°C]) are 0.65°C [0.04–1.76°C] and 0.63°C [–0.50–2.39°C], respectively, lower than raw projections (2.98°C [1.85–4.22°C] and 2.94°C [2.04–4.39°C]) for 2080–2099 under the intermediate-emission scenario. Approximately half model uncertainty is reduced after constraint. The land area (population) experiencing temperature extremes in our metric is 78% (85%) of the raw projections. Our results imply a lower impact of extreme heat than implied by current raw CMIP6 projections.

**Plain Language Summary** Changes in mean temperature and temperature extremes at regional scale under a warmer climate have received much attention due to the impact on the climate change adaptation and mitigation. However, currently, some of state-of-the-art climate models are "too warm" and overestimate the projected regional warming, due to sampling too many high climate sensitivities in the ensemble. Taking China as an example, Coupled Model Intercomparison Project Phase 6 (CMIP6) models project larger regional warming than previous CMIP model generations predicted. This study revises the raw projections of mean and extreme warming over China based on observed warming. First, we develop a hierarchical emergent constraint framework to obtain constrained global warming projections. We then estimate the mean temperature and temperature extremes over China by using the constrained global warming and observed local warming. Our metric of changes in mean temperature and temperature extremes are 0.65 and 0.63°C lower than the raw projections for the end of the 21st century under intermediate-emission scenario. Correspondingly, the land area (population) that will witness significant increase in temperature extremes relative to twice the local inter-model standard deviation is 78% (85%) of the raw projection. Therefore, the impact of extreme heat will be milder than climate projections from the underlying CMIP6 simulations imply.

## 1. Introduction

In response to anthropogenic greenhouse gases (GHGs), the global surface air temperature (GSAT) has increased rapidly in the twentieth century. Direct observations have revealed that the GSAT in the first two decades of the 21st century was 0.99°C (0.84–1.10°C) higher than that from 1850 to 1900 (Eyring et al., 2021; Gulev, 2021; IPCC, 2021b). Although recent warming is unequivocal, climate change is not uniform regionally (IPCC, 2013, 2021b). Since the 1850s, recently China has experienced a rapid warming of 1.38°C, which is higher than the simultaneous global warming (Gulev, 2021; Li & Sun, 2021). This observable warming has increased the frequency and intensity of extreme climate events (Xu et al., 2013; W. Zhang & Zhou, 2020; W. Zhang et al., 2022) and impacted both natural ecosystems and society (Doblas-Reyes et al., 2021; Ranasinghe et al., 2021; Schleussner et al., 2017; Xu et al., 2013; W. Zhang & Zhou, 2020). A reliable temperature projection over China is important for climate change adaptation and mitigation activities.

Climate system models are useful tools for understanding past climate change mechanisms and projecting possible future change under idealized emission assumptions (Eyring et al., 2016; Taylor et al., 2012; Zhou

**Software:** Ziming Chen
**Supervision:** Tianjun Zhou, Xiaolong Chen, Wenxia Zhang, Meng Zuo, Wenmin Man, Yun Qian
**Visualization:** Ziming Chen, Meng Zuo
**Writing – original draft:** Ziming Chen
**Writing – review & editing:** Tianjun Zhou, Xiaolong Chen, Wenxia Zhang, Meng Zuo, Wenmin Man, Yun Qian

et al., 2020). The multimodel means of the Coupled Model Intercomparison Project Phase 6 (CMIP6) models suggest that under low, intermediate and high emission scenarios, mean surface air temperatures over China (CSAT) would increase by 1.08, 2.79, and 5.62°C, respectively, in 2081–2100 relative to 1986–2005 (You et al., 2021). The most significant increases in temperature are projected for higher latitudes and elevations (Yang et al., 2021; Yao et al., 2019; You et al., 2021). Furthermore, many simulations over China have been performed using high-resolution regional climate models (RCMs) to provide more detailed projection information (N. Chen & Gao, 2019; Gao et al., 2012; Xu et al., 2013; D. Zhang & Gao, 2020). Based on the RCM projections, under medium and high emission scenarios, the annual CSAT would increase by approximately 2.4 and 4.6°C, respectively, relative to 1986–2005 (D. Zhang & Gao, 2020).

The current climate models still show limitations in performance, which may affect future projections. Most CMIP5 models underestimate the surface mean temperature trend when compared with observations (L. Chen & Frauenfeld, 2014). The CMIP6 models are generally better than the CMIP5 in reproducing the climatological spatial pattern and changes in temperature and precipitation over China. Nevertheless, some common biases, including cold biases and underestimation of the surface mean temperature trend, still exist (Xin et al., 2020; Yang et al., 2021; You et al., 2021). Some CMIP6 models, called "warm models," project a larger increase and wider range of GSAT because higher climate sensitivity is more prevalent in the CMIP6 models than in the CMIP5 models (Hausfather et al., 2022; Liang et al., 2020; Meehl et al., 2020; Palmer et al., 2021, 2023; Ribes et al., 2021; Tebaldi et al., 2021; Tokarska et al., 2020). Although recent studies have reported that based on GSAT warming, we can produce regional climate change projections (X. Chen & Zhou, 2016; Z. Chen et al., 2022; Goodwin et al., 2020; Greve et al., 2018; Osborn et al., 2018; Watterson, 2018), how the current existing projections are biased by the "warm model" issue remains unknown.

Recently, the emergent constraint (EC) technique, based on the physical link between a modeled, but observable, variable in the present day and a projected variable in the future climate system, has been developed and used to improve the reliability of future projections, assuming that the real world is interchangeable with the Earth system models (Brient, 2020; Caldwell et al., 2018; Hall et al., 2019; Klein & Hall, 2015; Sanderson et al., 2021). The present-day observed warming trend has been used to constrain the GSAT warming projections (Lee et al., 2021; Liang et al., 2020; Tokarska et al., 2020).

The constrained GSAT warming is useful for other climate quantities that scale well with GSAT change (Hu et al., 2021; Lee et al., 2021). The projections of local temperature and water availability over the Artic and Eurasian continents can be constrained by using the observed GSAT warming trend (Chai et al., 2022; Hu et al., 2021; Ribes et al., 2022). In addition, combining the observed evidence of global and regional warming can refine the regional projection assessment (Qasmi & Ribes, 2022; Ribes et al., 2022). In this study, we aim to constrain the mean and extreme temperature projections over China by using reliable observational data sets. The following questions will be addressed: (a) Can we develop an observational constraint to improve the reliability of regional temperature projections by using the constrained GSAT and regional warming? (b) How much land area and population will be affected by temperature extremes under the constrained projection?

## 2. Data and Methods

### 2.1. Observations and Model Simulations

To investigate the response of the mean and extreme CSAT in the observations, we use the homogenized gridded data set CN05.1 ranged from 1961 to 2020 with a spatial resolution of 0.25° × 0.25° (Wu & Gao, 2013). Besides, multiple long-term observational data sets are used (Text S1 in Supporting Information S1).

We use monthly (daily) data from 23 (18) CMIP6 models (Tables S1 and S2 in Supporting Information S1) in historical simulations and future projections under four combined scenarios of shared socioeconomic pathways and representative concentration pathways, viz., SSP1-2.6, SSP2-4.5, SSP3-7.0, and SSP5-8.5 scenarios (Eyring et al., 2016; O'Neill et al., 2016). We describe the results for the intermediate-emission scenario (SSP2-4.5), while we also show the results for other emission scenarios. Multiple available realizations for each model are used. All the data are regridded to 2.5° × 2.5° grids using first-order conservative interpolation. The baseline period is 1995–2014. Following the IPCC AR6 (IPCC, 2021b), three specific projection periods are examined and termed as the near term (2021–2040), midterm (2041–2060), and long term (2080–2099).

### 2.2. Emergent Constraint and Pattern Scaling for Regional Warming

We assume that the GSAT warming in the present day and projections simulated by the CMIP6 models are exchangeable with those in reality (Sanderson et al., 2021; Williamson & Sansom, 2019). To constrain the GSAT projections, we use the hierarchical emergent constraint framework, which accounts for the precision in observational data sets compared with the classic EC (Bowman et al., 2018), based on the physical link between future GSAT warming and the present-day GSAT warming trend based on data from 1981 to 2014 (Text S2 in Supporting Information S1).

The constrained GSAT change is useful for quantifying the uncertainty in changes in other climate variables scaling well with GSAT change (Lee et al., 2021; Tebaldi & Arblaster, 2014). Hence, using the constrained warming of the GSAT, we scale the regional mean and extreme warming over China (Text S3 in Supporting Information S1). The temperature extremes are represented by the maximum value for daily maximum temperature for each year (TXx, https://www.climdex.org/learn/indices/#index-TXx).

Local projected warming is driven by GSAT warming, and applying regional constraints can improve the reliability of constrained projections (Qasmi & Ribes, 2022; Ribes et al., 2022). To account for the local warming related to the local feedback, we further correct the local projected warming by using the local residual warming trend (Text S4 in Supporting Information S1). Unless otherwise noted, the projected warming over China is constrained by the observed GSAT trend and the local residual warming trend.

To investigate the skill of constrained projections for local warming, we apply a leave-one-out perfect model test. Following Hersbach (2000) and Brunner et al. (2020), to measure the constraint quality, we use the continuous ranked probability skill score (CRPSS), which is defined as the relative error between the distribution of constrained projections and pseudo-observation warming (Text S5 in Supporting Information S1). Conceptually, a low CRPSS suggests a high quality of constrained projections (Hersbach, 2000). In addition, we calculate the root-mean-square error (RMSE) between the constrained and pseudo-observation warming projections.

To account for the source of uncertainty in the constrained projection, we estimate the contribution of uncertainty resulting from the EC parameters, present-day and projected internal variability, and the uncertainty that cannot be explained by EC (Text S6 in Supporting Information S1) following Simpson et al. (2021).

## 3. Results

### 3.1. Raw Projected Warming Over China

We first examine the time series for annual mean and extreme CSAT from the raw multi-model mean (MMM) of CMIP6 models under different scenarios (Figure 1a). For the near term, the warming shows minor differences across four scenarios. The regional mean annual CSAT is projected to increase by 1.10°C (0.66–1.63°C for the 5th–95th ensemble range) and 1.23°C (0.77–1.89°C) in the intermediate (SSP2-4.5) and high (SSP5-8.5) emission scenarios, respectively, relative to 1995–2014 (Figure 1a and Table S3 in Supporting Information S1). For the midterm (2041–2060) and long term (2080–2099), a larger degree of warming will be seen over China as emissions increase. For the long term, the regional mean is projected to increase by 2.98°C (1.85–4.22°C) and 5.59°C (3.57–8.56°C) under SSP2-4.5 and SSP5-8.5, respectively. For the heat extreme, the warming magnitudes of the daytime hot extreme (TXx) are close to those of the annual-mean CSAT. In the near term, the regional mean TXx increase by 1.11°C (0.73–1.81°C) and 1.24°C (0.68–2.14°C) in SSP2-4.5 and SSP5-8.5 scenarios, respectively (Figure S1a and Table S3 in Supporting Information S1). In the long term, the TXx increase by 2.94°C (2.04–4.39°C) and 5.42°C (3.38–8.28°C) under SSP2-4.5 and SSP5-8.5 scenarios, respectively.

To examine the regional response over China, we show the spatial patterns of surface air temperature increases under four scenarios in the long-term projections (Figure S2 in Supporting Information S1). Although the warming magnitude increases with emission level in the four scenarios, the warming patterns are similar. The increase in the annual surface air temperature is higher over high latitudes and elevations (Tibetan Plateau) than in other regions. Over some regions in northeastern and northwestern China and the Tibetan Plateau, the mean estimates of annual surface air temperature will increase by more than 3 and 6°C under the SSP2-4.5 and SSP5-8.5 scenarios, respectively. For heat extremes, the increases in TXx show spatial patterns similar to those of the mean temperature (Figures S1b–S1e in Supporting Information S1), while the warming magnitudes of TXx are larger than those of the mean temperature over the Tibetan Plateau and central, northern and northwestern China in both the SSP2-4.5 and SSP5-8.5 scenarios.

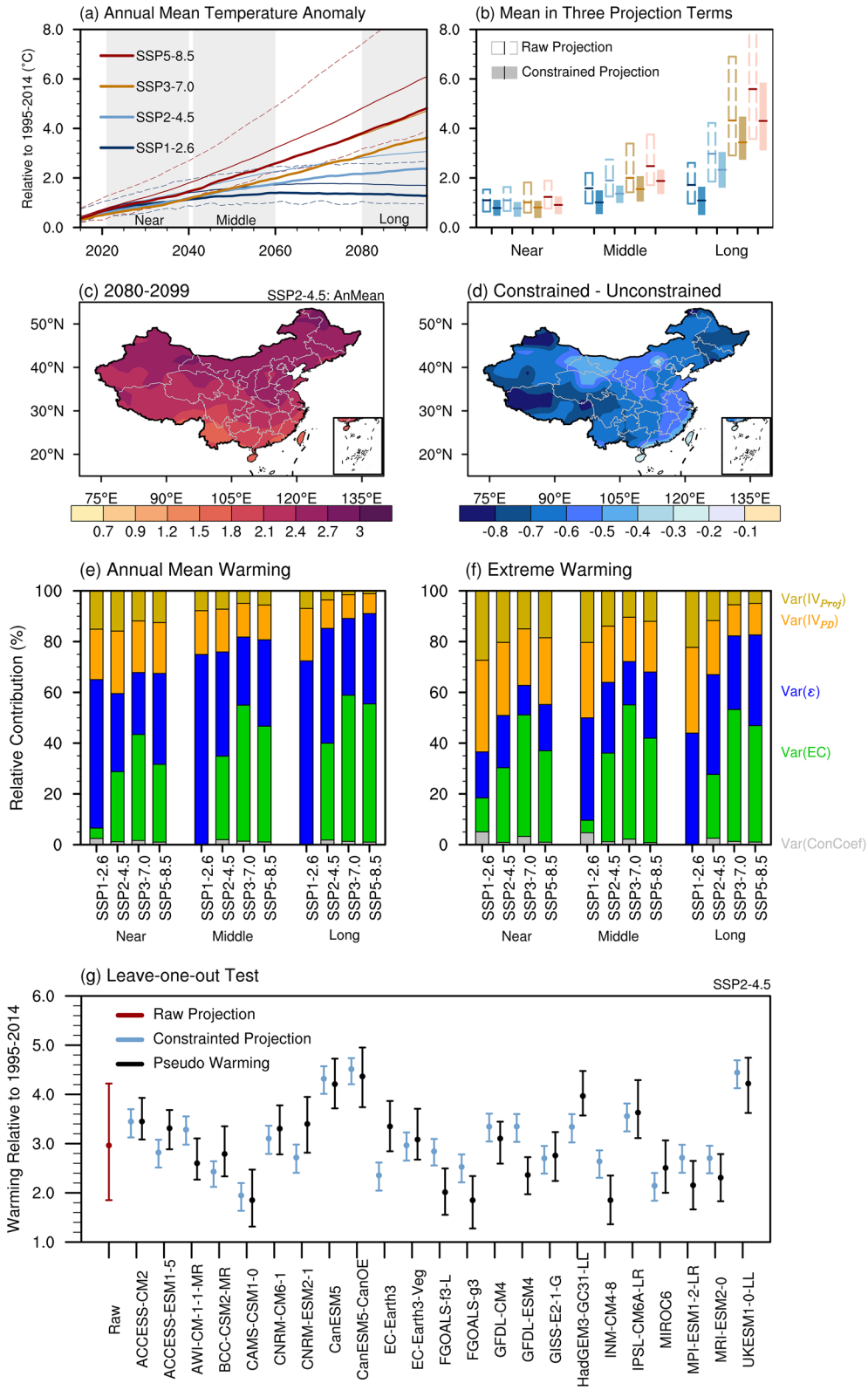


**Figure 1.**

While the CMIP6 models project warming in both the mean and extreme CSAT, there is a considerable spread among the projections. Here, we quantify the projection spread by using the very likely range, which is defined as the 5th and 95th ensemble ranges, following the IPCC (2021b). The very likely ranges of mean (extreme) CSAT increases are 1.85–4.22°C (2.04–4.39°C) and 3.57–8.56°C (3.38–8.28°C) in the long term under the SSP2-4.5 and SSP5-8.5 scenarios, respectively (Table S3 in Supporting Information S1). In addition, to assess the reliability of the results, we calculate the signal-to-noise ratio (SNR) between the absolute value of the projected changes and the projection spread. The SNRs of mean (extreme) CSAT increases are 1.26 (1.25) and 1.12 (1.11) in the long term, respectively, which means substantial inter-model uncertainties since the noise is almost equivalent to the signal.

### 3.2. Relationship Between Surface Air Temperature Warming Over China and GSAT Warming

We first examine the response of mean and extreme CSAT to global warming in the observations and show the spatial patterns of the regression coefficient between surface air temperature warming and GSAT for 1961–2020 (Figure S3 in Supporting Information S1). The observed warming over China is significantly well scaled with the GSAT, with a regional mean of 1.91°C/°C, indicating that the warming change in China is larger than the global average. The change in TXx is also scaled well with GSAT over most parts of China, and the spatial pattern is similar to that of the mean temperature.

We further extend our analysis to the projections. Both the mean and extreme warmings over China are significantly correlated with the GSAT increases across models under the SSP2-4.5 scenario (Figure 2). The projected regression pattern resembles the observation in the mean temperature. Analysis of the other three scenarios yielded similar conclusions (Figures S4–S6 in Supporting Information S1). For the heat extremes, the regression coefficient between TXx and GSAT is larger than that of mean warming over the Tibetan Plateau and central, eastern and southern China (Figures 2d–2f), indicating that the impact of extreme warming on these regions is larger than in other regions.

Since the CMIP6 models sample many high-climate-sensitivity models (Hausfather et al., 2022; IPCC, 2021a, 2021b), the raw projections of CMIP6 models may overestimate both the future mean and extreme warming over China. The relationship between the regional warming over China and the GSAT increase allows us to narrow down the model uncertainty for the projections by using the observationally constrained GSAT warming and the pattern scaling method shown below.

### 3.3. Observationally Constrained GSAT

To improve the reliability of the GSAT projections, we constrain the GSAT increases based on the inter-model relationship between the present-day warming trend and future warming. The present-day GSAT warming trend is associated with the global mean warming rate under a specific radiative forcing, that is, equilibrium climate sensitivity (ECS) (Tokarska et al., 2020). Hence, models with a higher ECS show larger warming magnitudes in both historical and future periods, as evinced by the significant correlation coefficients for the near term, midterm, and long term ($r = 0.80, 0.77, 0.74$, $p < 0.01$; Figure S7 in Supporting Information S1). Similar conclusions are found in the other three scenarios (Figure S8 in Supporting Information S1).

To constrain the projected GSAT increase, we calculate the mean GSAT trend based on three observational data sets (vertical dashed lines in Figure S7 in Supporting Information S1). Recent studies have indicated that a subset

**Figure 1.** *The annual mean surface air temperature warming over China (CSAT) in the raw and constrained projections relative to 1995–2014.* (a) The time series of the 10-year running CSAT warming. The thin solid lines are the multi-model means (MMMs) of CSAT warming, and the dashed lines represent the inter-model range of the 5th and 95th percentiles under SSP1-2.6 and SSP5-8.5. (b) The raw (hollow) and constrained (solid) projections of CSAT warming in three projection terms. The horizontal lines and the bars are the MMMs and inter-model ranges of the 5th and 95th percentiles, respectively. (c) The constrained warming patterns in the long term under SSP2-4.5 scenario. (d) Difference between constrained and raw projections. (e, f) The fraction of total variances in CSAT and TXx warming explained by the components of present-day (orange, Var($IV_{PD}$)) and projected internal variability (yellow, Var($IV_{Proj}$)), the emergent constraint (EC) (green, Var(EC)), the constraint coefficients (gray, Var(ConCoef)), and the inter-model differences in projections that are unrelated to the EC (blue, Var($\varepsilon$)) in CSAT and daily maximum temperature warming, respectively (Text S6 in Supporting Information S1). (g) The leave-one-out test perfect model test for the CSAT warming under SSP2-4.5. We remove the projected warming of the targeted model and set it as the pseudowarming (black) and then constrain the projected warming of the other model by using the present-day trend of the targeted model (blue) (Text S5 in Supporting Information S1). We also show the raw projections (red). The dots indicate the MMMs, while the vertical lines denote the range of the 5th and 95th percentiles. For the target model, the range is represented by the spread of the 5th and 95th percentiles of CSAT warming for 2080–2099.

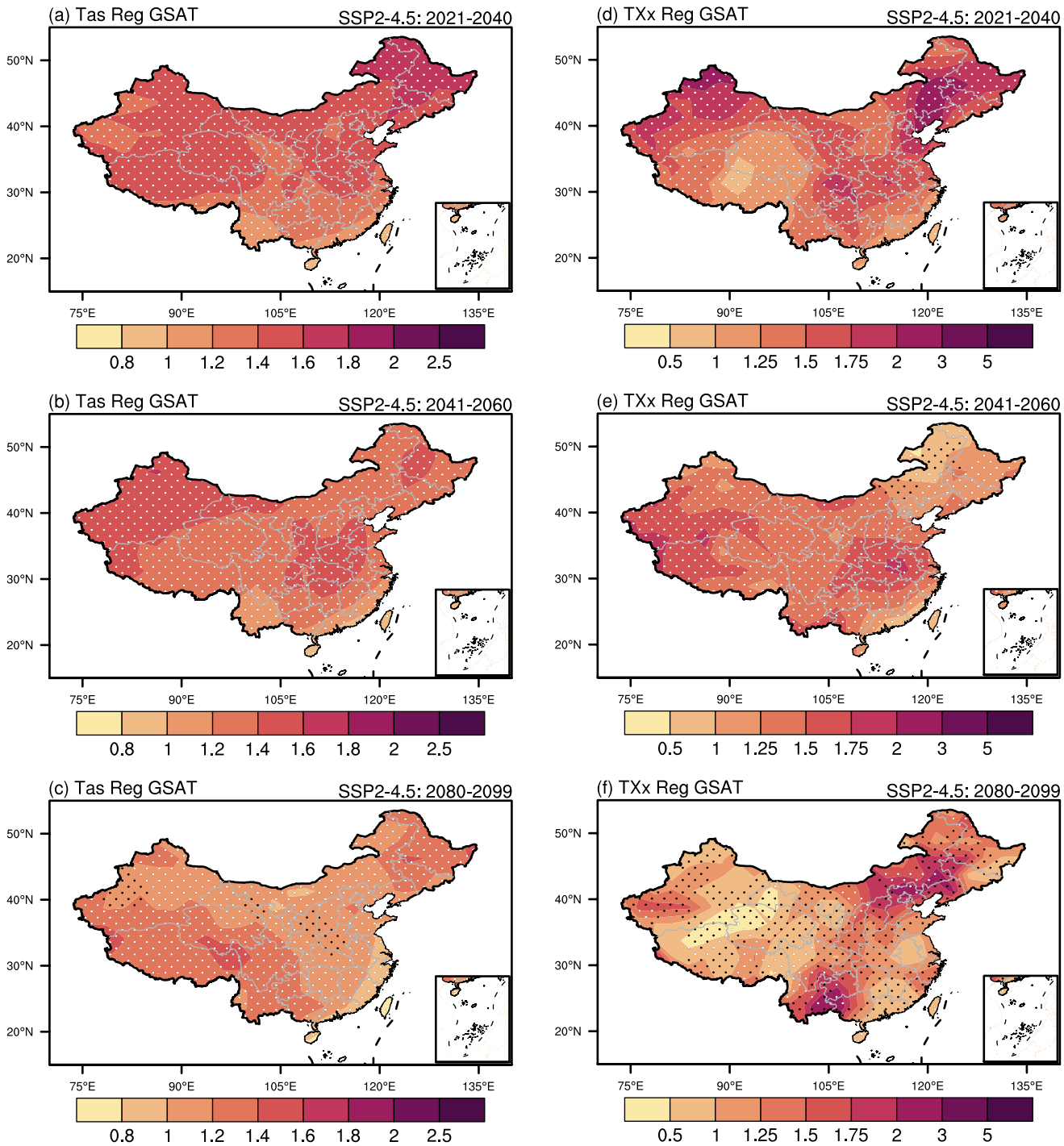


**Figure 2.** *The mean and extreme warming over China related to global surface air temperature* (*GSAT*) *warming*. (a–c) The increases in annual surface air temperature (Tas) and (d–f) daily maximum temperature (TXx) are regressed onto the concurrent GSAT warming in the (a, d) near term, (b, e) midterm, and (c, f) long term under the SSP2-4.5 scenario. We regress Tas and TXx onto GSAT for each model individually and then compute the multi-model mean. Black (white) stippling indicates that regression exceeds the 95% (99%) confidence level. Units: °C/°C

of CMIP6 models overestimate the present-day GSAT trend, leading to overestimation of the projected GAST warming (Liang et al., 2020; Tokarska et al., 2020). Our results show that the values of the GSAT trend simulated by most models are larger than the observations, indicating a systematic overestimation of the present-day GSAT trend by CMIP6 models. We show the correction for the constrained projections of GSAT for each model (Table

S4 in Supporting Information S1). The mean estimates of constrained GSAT warmings are 0.51°C (0.37–0.78°C), 0.92°C (0.72–1.40°C), and 1.50°C (1.12–2.46°C) in the near term, midterm, and long term under SSP2-4.5, respectively.

### 3.4. Constraint of the Projected Warming Over China

To identify how the uncertainty in the GSAT trend propagates to the projected CSAT warming, we show the inter-model relationship between the present-day GSAT trend and projected CSAT (TXx) warming in Figure S9 in Supporting Information S1 (Figure S10 in Supporting Information S1). Significant correlations between CSAT (TXx) and GSAT warming are seen at the 0.01 level under four emission scenarios. Since the models with higher climate sensitivity will simulate larger present-day GSAT trends, the projected GSAT warming and regional warming over China will be higher.

Based on the constrained GSAT warming and the inter-model relationship between projected warming over China and GSAT increase, we attain the constrained CSAT projections (Figure 1a and Table S3 in Supporting Information S1). In addition, to account for the warming related to the local feedback effect, we further constrain the local projected warming over the regions with a significant relationship between the projected warming constrained by GSAT and present-day residual warming (Text S4 and Figures S11–S14 in Supporting Information S1).

We assess the skill of the constrained projections through the leave-one-out perfect model test (Text S5 in Supporting Information S1). The results clearly indicate that the constrained projections exhibit a closer alignment with the pseudo warming compared to the raw projections (Figure 1g, Figures S15 and S16 in Supporting Information S1). The pseudowarming of the three leave-out models out of all the 23 models (~13% probability) fall completely outside the 5th–95th confidence range of the constrained projections under SSP2-4.5 (EC-Earth3, FGOALS-f3-L, GFDL-ESM4). When comparing the performance metrics, the constrained projections generally show lower RMSEs and CRPSSs than the raw projections, except for the constrained TXx projections under SSP1-2.6 (Figures S17 and S18 in Supporting Information S1). The largest reductions in RMSEs for constrained mean and TXx warming are seen in the long term under the SSP3-7.0 scenario, reaching −41% and −25%, respectively. Similarly, the reductions in CRPSSs are, respectively, −45% and −31% in the midterm and long term under the SSP3-7.0 scenario. Overall, the results from the leave-one-out perfect model test demonstrate the usefulness of the constrained projection.

The near-term constrained CSAT projections increase by 0.78–0.91°C and show small difference among scenarios. The constrained projections of warming in the midterm and long term will be larger as emission increase. The constrained CSAT projections in the long term increases by 2.33°C (1.61–3.05°C) under SSP2-4.5. The corresponding increases are 1.09°C (0.50–1.64°C) under SSP1-2.6, 3.44°C (2.74–4.48°C) under SSP3-7.0, and 4.30°C (3.12–5.85°C) under SSP5-8.5. Compared to the raw (or unconstrained) projections, the mean estimates of constrained projections show less warming, with the largest reduction of 1.29°C occurring in the long term under SSP5-8.5. The corresponding reduction after constraint is 0.63–0.88°C in the other three scenarios. In addition, the model uncertainties are also reduced after the EC, with a mean reduction in the inter-model variance by 38% in the long term under SSP2-4.5 (Table S3 in Supporting Information S1).

For the temperature extremes, the TXx increase in the constrained projections are also lower than that in the raw projections (Figure S1a and Table S3 in Supporting Information S1). The mean estimates of constrained TXx increase are 0.73–0.87°C in the near term and show small difference among scenarios. In the long term, the constrained projections of TXx increases by 1.32°C (0.43–1.99°C), 2.31°C (1.21–2.99°C), 3.26°C (2.25–4.61°C), and 4.22°C (2.83–5.81°C) under the SSP1-2.6, SSP2-4.5, SSP3-7.0, and SSP5-8.5 scenarios, respectively. In addition, the mean estimate of constrained TXx shows 1.20°C less warming than the raw projections in the long term under SSP5-8.5. The corresponding reductions in TXx after constraint are 0.36–1.02°C in the other three scenarios. The mean reduction in the inter-model variance is reduced by 25% in the long term under SSP2-4.5 (Table S3 in Supporting Information S1).

Regionally, the constrained warming is larger over high latitudes and elevations than that over other regions in China (Figures 1c and 1d). Relative to the raw MMM, substantial reductions are seen over 25°N north of China in the midterm (0.3–0.8°C) and long term (0.5–0.9°C) under SSP2-4.5 (Figure 1d and Figure S19 in Supporting Information S1). Similar results are seen in the SSP5-8.5 scenario (Figure S20 in Supporting Information S1).

For the temperature extremes, the patterns of TXx warming in the constrained projections are similar to those of mean warming (Figures S21 and S22 in Supporting Information S1), while the largest differences between constrained and unconstrained projections are seen over the Tibetan Plateau and central and south China. Relative

to the raw MMM of extreme warming, the reductions in TXx after the constraint are 0.1–1.0°C and 0.3–1.0°C in the midterm and long term under SSP2-4.5, respectively. The most substantial reduction exceeds 1.5°C over the Tibetan Plateau under SSP5-8.5 (Figure S22f in Supporting Information S1). Thus, the future extreme temperature warming will be milder than the raw CMIP6 projections.

To account for the reduced uncertainty resulting from the application of the EC, we examine the relative contribution of different uncertainty sources (Figures 1e and 1f). The results show that ∼28%, ∼33%, and ∼38% of the projection uncertainty in CSAT warming can be explained and reduced by the EC framework in the near term, midterm, and long term under SSP2-4.5, respectively (Table S3 in Supporting Information S1). Similarly, ∼29%, ∼35%, and ∼25% of the projection uncertainty in TXx warming is reduced. Given that the model uncertainty accounts for 60%–80% and 50%–64% in CSAT and TXx warming under SSP2-4.5, approximately half of the model uncertainty will be reduced after the EC. In addition, larger reductions in projection uncertainty are seen under SSP3-7.0 and SSP5-8.5. On the other hand, consistent with previous studies (Hawkins & Sutton, 2009; Lehner et al., 2020), the contribution of internal variability is important in the near term and decreases over time.

### 3.5. Impacts on the Population

Heat extremes are one of the most impact-relevant influences of a warmer climate, particularly for China, which is vulnerable to global warming and has a large population. Understanding the impacts and risks of TXx increase is critical for mitigation and adaptation planning. Here, we further estimate the extent of the land area and population impact of heat extremes in China.

To quantify the impacts on the areal extent in China, we examine the land fraction that will experience significant TXx warming (Figures 3a–3c; Text S7 in Supporting Information S1). In the constrained projections, the mean estimates of land fractions with significant TXx warming are 56% and 73% in the midterm and long term under SSP2-4.5, respectively, which are 64% and 78% of the raw projections. The constrained projections yield a lower land fraction affected by temperature extremes. Under SSP5-8.5, the land fraction with significant TXx warming will increase to 74% and 88% in the midterm and long term for the constrained projections, respectively (Figures S23 in Supporting Information S1), which are 18% and 15% higher than those under SSP2-4.5.

We further quantify the impacts on the population (Figures 3d–3f). In the midterm and long term, mean estimates of 56% and 84% of the population will be affected by the significant TXx warming under SSP2-4.5, representing 57% and 85% of the raw projections. Under SSP5-8.5, the population percentage affected by significant TXx warming will increase to 84% and 98% in the midterm and long term, respectively, for the constrained projections (Figures S23 in Supporting Information S1), with these increases being 28% and 14% higher than those under SSP2-4.5.

Hence, less land area and population in China will experience a significant increase in temperature extremes in the constrained projection.

## 4. Conclusion and Discussion

### 4.1. Conclusion

Global-scale warming is expected to continue under the continued emission of GHGs and will exert adverse impacts on natural ecosystems and human society through climate extremes (Doblas-Reyes et al., 2021; IPCC, 2021a, 2021b; Ranasinghe et al., 2021). The "warm model" problem of CMIP6 may lead to exaggerated projections at the regional scale. Here, we provide a solution for regional projections by taking China as an example. Based on a leave-one-out perfect model test, the performance of the constrained projections is confirmed to be higher than the raw projections under the intermediate-to-high emission scenarios. The major conclusions are summarized as follows:

1. We can constrain the CSAT projections based on the observationally constrained GSAT and the relationship between the regional warming and the GSAT, and can further correct the constrained warming based on the significant relationship between the constrained warming and present-day local residual trend. In the constrained projections, the mean estimates of mean and extreme CSAT averaged in 2080–2099 will be higher by 2.33°C and 2.31°C than those in 1995–2014 baseline period under the SSP2-4.5 scenario and 0.65°C and

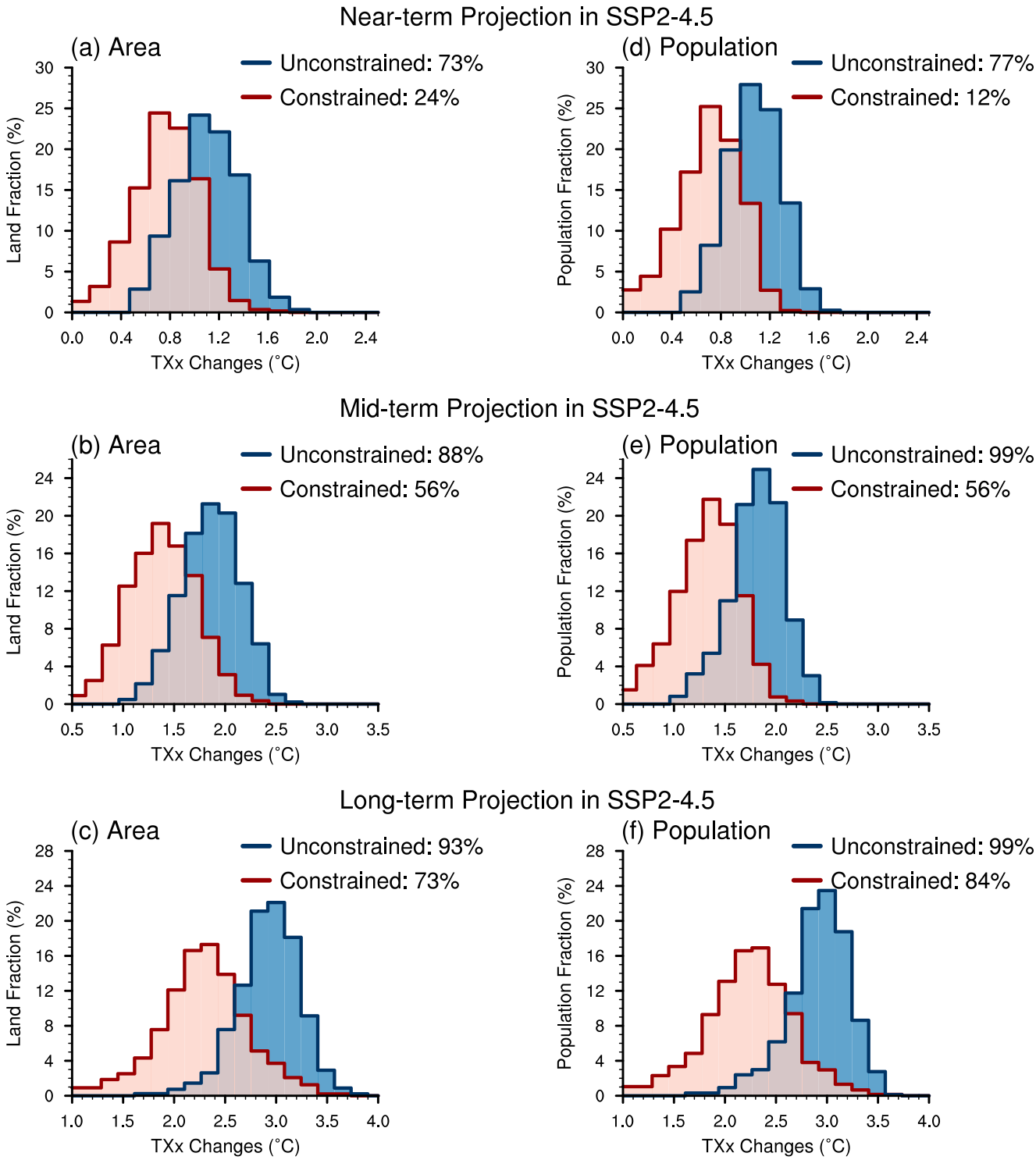


**Figure 3.** *The land and population fractions affected by temperature extremes over China*. (a–c) Spatial distribution and (d–f) population distribution of unconstrained (blue) and constrained (red) warming in TXx under the SSP2-4.5 scenario. The probability distribution functions (PDFs) are aggregated by the land area fraction that will experience certain TXx warming in the (a) near term, (b) midterm, and (c) long term. (d–f) Are the same as (a–c) but for the PDFs aggregated by the population fraction. The quantities in the legends are the land area fraction or population fraction, which will experience a significant increase in the unconstrained and constrained projections. A significant increase is defined as an increase that exceeds twice the local standard deviation across models (see Text S7 in Supporting Information S1).

0.63°C less than the raw CMIP6 projections, respectively. After the EC, approximately half of the model uncertainty will be reduced.

2. The land area and population that will experience a significant increase in extreme temperature in the constrained projections are less than the raw projections. In 2080–2099, the mean estimates of land and population fractions with significant TXx warming are 73% and 84%, respectively, under SSP2-4.5, that is, 78% and 85% of the raw projections. Under SSP5-8.5, the fractions will be 15% and 14% higher than those under SSP2-4.5.

### 4.2. Discussion

Given the inter-model spread in the constrained projections, we recognize the potential influence of other regional processes on the constrained CSAT and TXx warming. To explore these processes, we examine the inter-model statistical relationship between the regional metrics and the constrained warming over China, following the methods of Lorenz et al. (2018) (Table S6 in Supporting Information S1). The results reveal that after the EC using the GSAT and residual trends, the constrained mean and TXx warming over China do not exhibit significant correlations with most of the regional metrics, except for the present-day interannual variability of precipitation (prSTD) and sea level pressure (pslSTD). Notably, significant correlations are found between prSTD and constrained TXx warming under SSP1-2.6 and SSP2-4.5, and between pslSTD and constrained mean warming under SSP3-7.0 and SSP5-8.5. These findings suggest that the projected warming in the region may be influenced by climate variability, which is superimposed on long-term trends (Lorenz et al., 2018; Perkins & Fischer, 2013). In addition, under SSP1-2.6 scenario, significant correlations emerge between present-day surface temperature variability (tsSTD) and constrained CSAT warming, as well as between tsSTD and constrained TXx warming. These correlations indicate that models exhibiting larger positive biases in present-day temperature variability tend to overestimate warming in the projections (Christensen & Boberg, 2012). Therefore, careful consideration should be given to the selection of regional metrics when further constraining regional warming. After constraining the regional warming by using GSAT, it is necessary to investigate which regional metrics can provide further constraints on the regional warming.

At the global scale, climate sensitivities may be suppressed by the observed enhanced zonal SST gradient in the tropical Pacific resulting from internal variability or radiative forcing (Hartmann, 2022; Seager et al., 2022; Watanabe et al., 2021). The impacts of low-likelihood high-warming (LLHW) events simulated by high-climate-sensitivity models may emerge as the pattern effect diminishes and ozone recovers (Sherwood et al., 2020). Based on the findings of the leave-one-out method analysis, it is anticipated that the projected CSAT warming would deviate from the constrained (5th–95th percentile) range in about 1 out of 10 instances (~13% probability) under the SSP2-4.5 scenario. In addition, Palmer et al. (2023) reported that many high-climate-sensitivity models can capture the key large-scale processes that are important for representing the European climate. Hence, we could not rule out the probability of LLHW storylines projected by high-climate-sensitivity models (Hausfather et al., 2022; Lee et al., 2021; Palmer et al., 2023). Focusing on the LLHW storyline (Table S7 in Supporting Information S1), the constrained warmings are still lower than the raw projections. So the impact of the "warm model" should be taken into account when making risk-averse policies.

Our results will provide a useful reference for future adaptation and mitigation in China. Besides, the technique employed, such as EC and leave-one-out testing, can be helpful to other parts of the world in tackling the CMIP6 "warm model" problem to develop reliable regional climate change projections.

## Data Availability Statement

The data supporting the findings are freely available. Berkeley Earth Surface Temperature are available from NCAR Climate Data Guide (https://climatedataguide.ucar.edu/climate-data/global-surface-temperatures-best-berkeley-earth-surface-temperatures). Surface temperature data set of NASA Goddard Institute for Space Studies is available from https://data.giss.nasa.gov/gistemp/. Surface temperature data set of Cowtan and Way is available from https://www-users.york.ac.uk/~kdc3/papers/coverage2013/series.html. The data is analyzed with NCL (http://www.ncl.ucar.edu/). The code used to produce the results are available from https://github.com/Steven04453X/Emergent-constraint-projection-of-mean-and-extreme-warming-in-China.git. The data of the results are available from https://github.com/Steven04453X/Emergent-constrained-projections-of-mean-and-extreme-warming-in-China.git.

**Acknowledgments**
This study is supported by the National Natural Science Foundation of China (Grant 41988101), National Key Research and Development Program of China (2020YFA0608904), and the Second Tibetan Plateau Scientific Expedition and Research (STEP) program (Grant 2019QZKK0102). This research is also supported by the US Department of Energy (DOE), Office of Science, Office of Biological and Environmental Research (BER), as part of the Global and Regional Model Analysis program area. The Pacific Northwest National Laboratory (PNNL) is operated for the DOE by the Battelle Memorial Institute under Contract DE-AC05-76RLO1830. We also acknowledge the support from Jiangsu Collaborative Innovation Center for Climate Change and Dr. Jian Lu. We thank WCRP's WGCM for making available CMIP6 model output (Tables S1 and S2 in Supporting Information S1) (https://esgf-node.llnl.gov/search/cmip6/), and NOAA/OAR/ESRL PSD for providing the NOAA merged land ocean global surface temperature data sets (https://www.ncei.noaa.gov/products/land-based-station/noaa-global-temp).

## References

Bowman, K. W., Cressie, N., Qu, X., & Hall, A. (2018). A hierarchical statistical framework for emergent constraints: Application to snow-albedo feedback. *Geophysical Research Letters*, *45*(23), 13050–13059. https://doi.org/10.1029/2018gl080082

Brient, F. (2020). Reducing uncertainties in climate projections with emergent constraints: Concepts, examples and prospects. *Advances in Atmospheric Sciences*, *37*(1), 1–15. https://doi.org/10.1007/s00376-019-9140-8

Brunner, L., Pendergrass, A. G., Lehner, F., Merrifield, A. L., Lorenz, R., & Knutti, R. (2020). Reduced global warming from CMIP6 projections when weighting models by performance and independence. *Earth System Dynamics*, 1–24. https://doi.org/10.5194/esd-2020-23

Caldwell, P. M., Zelinka, M. D., & Klein, S. A. (2018). Evaluating emergent constraints on equilibrium climate sensitivity. *Journal of Climate*, *31*(10), 3921–3942. https://doi.org/10.1175/jcli-d-17-0631.1

Chai, Y., Yue, Y., Slater, L. J., Yin, J., Borthwick, A. G. L., Chen, T., & Wang, G. (2022). Constrained CMIP6 projections indicate less warming and a slower increase in water availability across Asia. *Nature Communications*, *13*(1), 1–9. https://doi.org/10.1038/s41467-022-31782-7

Chen, L., & Frauenfeld, O. W. (2014). Surface air temperature changes over the twentieth and twenty-first centuries in China simulated by 20 CMIP5 models. *Journal of Climate*, *27*(11), 3920–3937. https://doi.org/10.1175/JCLI-D-13-00465.1

Chen, N., & Gao, X. (2019). Climate change in the twenty-first century over China: Projections by an RCM and the driving GCM. *Atmospheric and Oceanic Science Letters*, *12*(4), 270–277. https://doi.org/10.1080/16742834.2019.1612695

Chen, X., & Zhou, T. (2016). Uncertainty in crossing time of 2°C warming threshold over China. *Science Bulletin*, *61*(18), 1451–1459. https://doi.org/10.1007/s11434-016-1166-z

Chen, Z., Zhou, T., Chen, X., Zhang, W., Zhang, L., Wu, M., & Zou, L. (2022). Observationally constrained projection of Afro-Asian monsoon precipitation. *Nature Communications*, *13*(1), 1–12. https://doi.org/10.1038/s41467-022-30106-z

Christensen, J. H., & Boberg, F. (2012). Temperature dependent climate projection deficiencies in CMIP5 models. *Geophysical Research Letters*, *39*(24), 1–5. https://doi.org/10.1029/2012GL053650

Doblas-Reyes, F. J., Sörensson, A. A., Almazroui, M., Dosio, A., Gutowski, W. J., Haarsma, R., et al. (2021). Chapter 10: Linking global to regional climate change. In V. Masson-Delmotte, P. Zhai, A. Pirani, S. L. Connors, C. Péan, S. Berger, et al. (Eds.), *Climate change 2021: The physical science basis. Contribution of working group I to the sixth assessment report of the intergovernmental panel on climate change*. Cambridge University Press. https://doi.org/10.1007/978-3-319-76

Eyring, V., Bony, S., Meehl, G. A., Senior, C. A., Stevens, B., Stouffer, R. J., & Taylor, K. E. (2016). Overview of the coupled model intercomparison project phase 6 (CMIP6) experimental design and organization. *Geoscientific Model Development*, *9*(5), 1937–1958. https://doi.org/10.5194/gmd-9-1937-2016

Eyring, V., Gillett, N. P., Achuta Rao, K. M., Barimalala, R., Barreiro Parrillo, M., Bellouin, N., et al. (2021). Chapter 3: Human influence on the climate system. In V. Masson-Delmotte, P. Zhai, A. Pirani, S. L. Connors, C. Péan, S. Berger, et al. (Eds.), *Climate change 2021: The physical science basis. Contribution of working group I to the sixth assessment report of the intergovernmental panel on climate change (Masson-Del)*. Cambridge University Press. https://doi.org/10.1002/2014GL06106

Gao, X., Shi, Y., Zhang, D., & Giorgi, F. (2012). Climate change in China in the 21st century as simulated by a high resolution regional climate model. *Chinese Science Bulletin*, *57*(10), 1188–1195. https://doi.org/10.1007/s11434-011-4935-8

Goodwin, P., Leduc, M., Partanen, A. I., Damon Matthews, H., & Rogers, A. (2020). A computationally efficient method for probabilistic local warming projections constrained by history matching and pattern scaling, demonstrated by WASP-LGRTC-1.0. *Geoscientific Model Development*, *13*(11), 5389–5399. https://doi.org/10.5194/gmd-13-5389-2020

Greve, P., Gudmundsson, L., & Seneviratne, S. I. (2018). Regional scaling of annual mean precipitation and water availability with global temperature change. *Earth System Dynamics*, *9*(1), 227–240. https://doi.org/10.5194/esd-9-227-2018

Gulev, S. K. (2021). Chapter 2: Changing state of the climate system. In *Climate change 2021: The physical science basis. Contribution of working group I to the sixth assessment report of the intergovernmental panel on climate change*. Cambridge University Press.

Hall, A., Cox, P., Huntingford, C., & Klein, S. (2019). Progressing emergent constraints on future climate change. *Nature Climate Change*, *9*(4), 269–278. https://doi.org/10.1038/s41558-019-0436-6

Hartmann, D. L. (2022). The Antarctic ozone hole and the pattern effect on climate sensitivity. *Proceedings of the National Academy of Sciences of the United States of America*, *119*(35), 1–5. https://doi.org/10.1073/pnas.2207889119

Hausfather, Z., Marvel, K., Schmidt, G. A., Nielsen-gammon, J. W., & Zelinka, M. (2022). Climate simulations: Recognize the 'hot model' problem. *Nature*, *605*(7908), 26–29. https://doi.org/10.1038/d41586-022-01192-2

Hawkins, E., & Sutton, R. (2009). The potential to narrow uncertainty in regional climate predictions. *Bulletin of the American Meteorological Society*, *90*(8), 1095–1108. https://doi.org/10.1175/2009bams2607.1

Hersbach, H. (2000). Decomposition of the continuous ranked probability score for ensemble prediction systems. *Weather and Forecasting*, *15*(5), 559–570. https://doi.org/10.1175/1520-0434(2000)015<0559:DOTCRP>2.0.CO;2

Hu, X. M., Ma, J. R., Ying, J., Cai, M., & Kong, Y. Q. (2021). Inferring future warming in the Arctic from the observed global warming trend and CMIP6 simulations. *Advances in Climate Change Research*, *12*(4), 499–507. https://doi.org/10.1016/j.accre.2021.04.002

IPCC. (2013). Summary for policymakers. In T. F. Stocker, D. Qin, G.-K. Plattner, M. Tignor, S. K. Allen, et al. (Eds.), *Climate change 2013: The physical science basis. Contribution of working group I to the fifth assessment report of the intergovernmental panel on climate change*. Cambridge University Press.

IPCC. (2021a). In V. Masson-Delmotte, P. Zhai, A. Pirani, S. L. Connors, C. Péan, et al. (Eds.), *The physical science basis. Contribution of working group I to the sixth assessment report of the intergovernmental panel on climate change*. Cambridge University Press. https://doi.org/10.1017/9781009157896

IPCC. (2021b). Summary for policymakers. In V. Masson-Delmotte, P. Zhai, A. Pirani, S. L. Connors, C. Péan, et al. (Eds.), *Climate change 2021: The physical science basis. Contribution of working group I to the sixth assessment report of the intergovernmental panel on climate change* (p. 42). Cambridge University Press. Retrieved from https://www.ipcc.ch/report/ar6/wg1/

Klein, S. A., & Hall, A. (2015). Emergent constraints for cloud feedbacks. *Current Climate Change Reports*, *1*(4), 276–287. https://doi.org/10.1007/s40641-015-0027-1

Lee, J. Y., Marotzke, J., Bala, G., Cao, L., Corti, S., Dunne, J. P., et al. (2021). Chapter 4: Future global climate: Scenario-based projections and near-term information. In V. Masson-Delmotte, P. Zhai, A. Pirani, S. L. Connors, C. Péan, S. Berger, et al. (Eds.), *Climate change 2021: The physical science basis. Contribution of working group I to the sixth assessment report of the intergovernmental panel on climate change*. Cambridge University Press.

Lehner, F., Deser, C., Maher, N., Marotzke, J., Fischer, E. M., Brunner, L., et al. (2020). Partitioning climate projection uncertainty with multiple large ensembles and CMIP5/6. *Earth System Dynamics*, *11*(2), 491–508. https://doi.org/10.5194/esd-11-491-2020

Li, Q., & Sun, W. (2021). China global merged surface temperature data set (CMST-Interim) - Upgraded version. *PANGAEA*. https://doi.org/10.1594/PANGAEA.929389

Liang, Y., Gillett, N. P., & Monahan, A. H. (2020). Climate model projections of 21st century global warming constrained using the observed warming trend. *Geophysical Research Letters*, *47*(12), e2019GL086757. https://doi.org/10.1029/2019gl086757

Lorenz, R., Herger, N., Sedláček, J., Eyring, V., Fischer, E. M., & Knutti, R. (2018). Prospects and caveats of weighting climate models for summer maximum temperature projections over North America. *Journal of Geophysical Research: Atmospheres*, *123*(9), 4509–4526. https://doi.org/10.1029/2017JD027992

Meehl, G. A., Senior, C. A., Eyring, V., Gregory, F., Lamarque, J.-F., Stouffer, R. J., et al. (2020). Context for interpreting equilibrium climate sensitivity and transient climate response from the CMIP6 Earth system models. *Science Advances*, *6*(26), eaba1981. https://doi.org/10.1126/sciadv.aba1981

O'Neill, B. C., Tebaldi, C., van Vuuren, D. P., Eyring, V., Friedlingstein, P., Hurtt, G., et al. (2016). The scenario model Intercomparison project (ScenarioMIP) for CMIP6. *Geoscientific Model Development*, *9*(9), 3461–3482. https://doi.org/10.5194/gmd-9-3461-2016

Osborn, T. J., Wallace, C. J., Lowea, J. A., & Bernie, D. (2018). Performance of pattern-scaled climate projections under high-end warming. Part I: Surface air temperature over land. *Journal of Climate*, *31*(14), 5667–5680. https://doi.org/10.1175/JCLI-D-17-0780.1

Palmer, T. E., Booth, B. B. B., & McSweeney, C. F. (2021). How does the CMIP6 ensemble change the picture for European climate projections? *Environmental Research Letters*, *16*(9), 094042. https://doi.org/10.1088/1748-9326/ac1ed9

Palmer, T. E., McSweeney, C. F., Booth, B. B. B., Priestley, M. D. K., Davini, P., Brunner, L., et al. (2023). Performance based sub-selection of CMIP6 models for impact assessments in Europe. *Earth System Dynamics Discussions*, *14*(2), 457–483. https://doi.org/10.5194/esd-2022-31%0A

Perkins, S. E., & Fischer, E. M. (2013). The usefulness of different realizations for the model evaluation of regional trends in heat waves. *Geophysical Research Letters*, *40*(21), 5793–5797. https://doi.org/10.1002/2013GL057833

Qasmi, S., & Ribes, A. (2022). Reducing uncertainty in local temperature projections. *Science Advances*, *8*(41), 1–14. https://doi.org/10.1126/sciadv.abo6872

Ranasinghe, R., Ruane, A. C., Vautard, R., Arnell, N., Coppola, E., Cruz, F. A., et al. (2021). Chapter 12: Climate change information for regional impact and for risk assessment. In V. Masson-Delmotte, P. Zhai, A. Pirani, S. L. Connors, C. Péan, S. Berger, et al. (Eds.), *Climate change 2021: The physical science basis. Contribution of working group I to the sixth assessment report of the intergovernmental panel on climate change*. Cambridge University Press.

Ribes, A., Boé, J., Qasmi, S., Dubuisson, B., Douville, H., & Terray, L. (2022). An updated assessment of past and future warming over France based on a regional observational constraint. *Earth System Dynamics*, *13*(4), 1397–1415. https://doi.org/10.5194/esd-13-1397-2022

Ribes, A., Qasmi, S., & Gillett, N. P. (2021). Making climate projections conditional on historical observations. *Science Advances*, *7*(4), eabc0671. https://doi.org/10.1126/sciadv.abc0671

Sanderson, B. M., Pendergrass, A. G., Koven, C. D., Brient, F., Booth, B. B. B., Fisher, R. A., & Knutti, R. (2021). The potential for structural errors in emergent constraints. *Earth System Dynamics*, *12*(3), 899–918. https://doi.org/10.5194/esd-12-899-2021

Schleussner, C.-F., Pfleiderer, P., & Fischer, E. M. (2017). In the observational record half a degree matters. *Nature Climate Change*, *7*(7), 460–462. https://doi.org/10.1038/nclimate3320

Seager, R., Henderson, N., & Cane, M. (2022). Persistent discrepancies between observed and modeled trends in the tropical Pacific Ocean. *Journal of Climate*, *35*(14), 4571–4584. https://doi.org/10.1175/JCLI-D-21-0648.1

Sherwood, S. C., Webb, M. J., Annan, J. D., Armour, K. C., Forster, P. M., Hargreaves, J. C., et al. (2020). An assessment of Earth's climate sensitivity using multiple lines of evidence. *Reviews of Geophysics*, *58*(4), 1–92. https://doi.org/10.1029/2019RG000678

Simpson, I. R., McKinnon, K. A., Davenport, F. V., Tingley, M., Lehner, F., Al Fahad, A., & Chen, D. (2021). Emergent constraints on the large-scale atmospheric circulation and regional hydroclimate: Do they still work in CMIP6 and how much can they actually constrain the future? *Journal of Climate*, *34*(15), 6355–6377. https://doi.org/10.1175/JCLI-D-21-0055.1

Taylor, K. E., Stouffer, R. J., & Meehl, G. A. (2012). An overview of CMIP5 and the experiment design. *Bulletin of the American Meteorological Society*, *93*(4), 485–498. https://doi.org/10.1175/bams-d-11-00094.1

Tebaldi, C., & Arblaster, J. M. (2014). Pattern scaling: Its strengths and limitations, and an update on the latest model simulations. *Climatic Change*, *122*(3), 459–471. https://doi.org/10.1007/s10584-013-1032-9

Tebaldi, C., Debeire, K., Eyring, V., Fischer, E., Fyfe, J., Friedlingstein, P., et al. (2021). Climate model projections from the scenario model Intercomparison project (ScenarioMIP) of CMIP6. *Earth System Dynamics*, *12*(1), 253–293. https://doi.org/10.5194/esd-12-253-2021

Tokarska, K. B., Stolpe, M. B., Sippel, S., Frischer, E. M., Smith, C. J., Lehner, F., & Knutti, R. (2020). Past warming trend constrains future warming in CMIP6 models. *Science Advances*, *6*(12), eaaz9549. https://doi.org/10.1126/sciadv.aaz9549

Watanabe, M., Dufresne, J. L., Kosaka, Y., Mauritsen, T., & Tatebe, H. (2021). Enhanced warming constrained by past trends in equatorial Pacific sea surface temperature gradient. *Nature Climate Change*, *11*(1), 33–37. https://doi.org/10.1038/s41558-020-00933-3

Watterson, I. G. (2018). Indices of climate change based on patterns from CMIP5 models, and the range of projections. *Climate Dynamics*, *52*(3–4), 2451–2466. https://doi.org/10.1007/s00382-018-4260-x

Williamson, D. B., & Sansom, P. P. G. (2019). How are emergent constraints quantifying uncertainty and what do they leave behind? *Bulletin of the American Meteorological Society*, *100*(12), 2571–2587. https://doi.org/10.1175/BAMS-D-19-0131.1

Wu, J., & Gao, X. (2013). A gridded daily observation data set over China region and comparison with the other data sets. *Chinese Journal of Geophysics*, *56*(4), 1102–1111. https://doi.org/10.6038/CJG20130406

Xin, X., Wu, T., Zhang, J., Yao, J., & Fang, Y. (2020). Comparison of CMIP6 and CMIP5 simulations of precipitation in China and the East Asian summer monsoon. *International Journal of Climatology*, *40*(15), 6423–6440. https://doi.org/10.1002/joc.6590

Xu, J., Shi, Y., Gao, X., & Giorgi, F. (2013). Projected changes in climate extremes over China in the 21st century from a high resolution regional climate model (RegCM3). *Chinese Science Bulletin*, *58*(12), 1443–1452. https://doi.org/10.1007/s11434-012-5548-6

Yang, X., Zhou, B., Xu, Y., & Han, Z. (2021). CMIP6 evaluation and projection of temperature and precipitation over China. *Advances in Atmospheric Sciences*, *38*(5), 817–830. https://doi.org/10.1007/s00376-021-0351-4

Yao, T., Xue, Y., Chen, D., Chen, F., Thompson, L., Cui, P., et al. (2019). Recent third pole's rapid warming accompanies cryospheric melt and water cycle intensification and interactions between monsoon and environment: Multidisciplinary approach with observations, modeling, and analysis. *Bulletin of the American Meteorological Society*, *100*(3), 423–444. https://doi.org/10.1175/bams-d-17-0057.1

You, Q., Cai, Z., Wu, F., Jiang, Z., Pepin, N., & Shen, S. S. P. (2021). Temperature data set of CMIP6 models over China: Evaluation, trend and uncertainty. *Climate Dynamics*, *57*(1–2), 17–35. https://doi.org/10.1007/s00382-021-05691-2

Zhang, D., & Gao, X. (2020). Climate change of the 21st century over China from the ensemble of RegCM4 simulations (in Chinese). *Chinese Science Bulletin*, *65*(23), 2516–2526. https://doi.org/10.1360/TB-2020-0231

Zhang, W., Furtado, K., Zhou, T., Wu, P., & Chen, X. (2022). Constraining extreme precipitation projections using past precipitation variability. *Nature Communications*, *13*(1), 1–11. https://doi.org/10.1038/s41467-022-34006-0

Zhang, W., & Zhou, T. (2020). Increasing impacts from extreme precipitation on population over China with global warming. *Science Bulletin*, *65*(3), 243–252. https://doi.org/10.1016/j.scib.2019.12.00

Zhou, T., Chen, Z., Zou, L., Chen, X., Yu, Y., Wang, B., et al. (2020). Development of climate and Earth system models in China: Past achievements and new CMIP6 results. *Journal of Meteorological Research*, *34*(1), 1–19. https://doi.org/10.1007/s13351-020-9164-0